Uncertainties in atmospheric neutrino fluxes

G. D. Barr[*] and S. Robbins[†]

Department of Physics, University of Oxford, Denys Wilkinson Building, Keble Road, Oxford, UK, OX1 3RH

T. K. Gaisser and T. Stanev

Bartol Research Institute and Department of Physics and Astronomy, University of Delaware, Newark, Delaware, USA 19716

An evaluation of the principal uncertainties in the computation of neutrino fluxes produced in cosmic ray showers in the atmosphere is presented. The neutrino flux predictions are needed for comparison with experiment to perform neutrino oscillation studies. The paper concentrates on the main limitations which are due to hadron production uncertainties. It also treats primary cosmic ray flux uncertainties, which are at a lower level. The absolute neutrino fluxes are found to have errors of around 15% in the neutrino energy region important for contained events underground. Large cancellations of these errors occur when ratios of fluxes are considered, in particular, the $\nu_\mu/\bar{\nu}_\mu$ ratio below $E_\nu = 1$ GeV, the $(\nu_\mu + \bar{\nu}_\mu)/(\nu_e + \bar{\nu}_e)$ ratio below $E_\nu = 10$ GeV and the up/down ratios above $E_\nu = 1$ GeV are at the 1% level. A detailed breakdown of the origin of these errors and cancellations is presented.

PACS numbers: 13.85.Tp, 14.60.Pq, 96.50.S−

I. INTRODUCTION

The Super-Kamiokande collaboration have published detailed analyses [1,2] of neutrino oscillation effects based on over 15 000 observed events induced by atmospheric neutrinos. Neutrino oscillations have also been observed in other measurements with atmospheric neutrinos [3–6], accelerator neutrinos [7], solar neutrinos [8,9] and reactor neutrinos [10]. A crucial part of the study of oscillation effects with atmospheric neutrinos is a detailed knowledge of the atmospheric neutrino beam at production, before oscillations occur. Increasingly sophisticated calculations [11–20] have appeared recently. The uncertainties on the calculated flux become a limiting factor when one uses the atmospheric neutrino beam to search for subleading effects such as θ_{13} mixing, submaximal mixing in the "atmospheric" sector or effects of solar mixing [21,22]. This paper reports on a study to enumerate the uncertainties in the neutrino fluxes due to the major sources of uncertainty in the input to these calculations.

The main features of the atmospheric neutrino fluxes can be understood from a discussion of their production mechanism as follows. Cosmic rays (about 80% of nucleons are free protons, the rest arrive bound in nuclei) collide with air molecules high in the atmosphere, generating mesons which subsequently decay. The main production of neutrinos occurs in the decay of charged pions $\pi^+ \rightarrow \mu^+ \nu$ and the subsequent decay of the muon $\mu^+ \rightarrow e^+ \bar{\nu}_\mu \nu_e$ (and similar for antiparticles starting with π^-). Decay schemes involving kaons also contribute to the higher energy neutrino fluxes. From the main production mechanism, it is easy to see that at low energy where

muons decay before hitting the earth, there should be roughly two muon type neutrinos for every electron type neutrino (this is quite a good rule of thumb, because the neutrino from the pion decay is similar in energy to the other neutrinos due to the heavy muon).

In practice, neutrino fluxes are computed using Monte-Carlo simulation in which the development of the cosmic ray cascade is followed step-by-step for each track to include details of bending in the Earth's magnetic field, of the density profile of the atmosphere and of particle energy loss. The influence of the Earth's magnetic field on the primary cosmic ray flux is included using a particle backtracking technique to evaluate the cutoffs (see e.g. [20]). This affects mostly primaries up to about 20 GeV. The primary cosmic ray flux in the same energy range is also modulated by the solar wind which varies with the 11-year solar cycle.

The Earth's magnetic field causes the main dependence of the fluxes on the location on the Earth, and also produces zenith and azimuth angle variation at each position. The zenith angle distribution is also affected by two other effects. (a) Higher energy muons hit the Earth's surface and stop before decay. This happens for vertical muons with energy above ∼3 GeV which have a path length of about 20 km. Path lengths up to 500 km are possible for horizontal muons and so higher energy neutrinos from muon decay are present in the horizontal fluxes. (b) The competition between meson decay and interaction occurs between 100 and 1000 GeV meson energy, with higher energy particles preferring interaction due to time dilation making decay less likely. Since more horizontal showers develop higher up, where the density is less, this crossover happens at higher energies than for vertical cosmic rays.

A complication [13,23] which is dealt with in modern Monte-Carlo calculations is the lateral spreading of the cosmic ray showers both from transverse momentum ac-

---

[*]Electronic address: giles.barr@physics.ox.ac.uk
[†]Now at Bergische Universität Wuppertal, Department of Physics, D-42097 Wuppertal, Germany

quired in the interactions and decay of mesons and from bending of muons in the Earth's magnetic field. This makes the computation awkward as it requires generation of particles in all directions at all points on the Earth. The geomagnetic field is not symmetric enough to be useful for simplifying the problem. A speed up trick which can be used with care is to extend the size of the detector to cover an area extending ~500 km around the detector [20]. A much larger detector increases significantly the number of useful air showers.

Early calculations [11,12] used a "1-dimensional" (1D) approximation in which the direction of decay and inter-action products are adjusted to lie along the trajectory of the primary particle at its point of first collision. In this approximation, bending of secondaries in the geomagnetic field is neglected. This allows the calculation to consider only trajectories that point directly at the detector, considerably reducing the computation time (by about a factor of 100 in the calculation in Ref. [20]). One effect of making the 1D approximation is that a geometric enhancement of sub-GeV neutrino fluxes near the horizon [13,23] is neglected. Charge-sign dependence of muon bending in the geomagnetic field produces differences between neutrinos and antineutrinos up to ~100 GeV [23] which are absent in the 1D approximation. Both effects are difficult to see with current detectors; the first because of the poor correlation at low energy between the direction of the neutrino and that of the charged lepton it produces, and the second because of the difficulty of measuring the charge of the neutrino-induced lepton. The geometric effect has been found to affect only neutrinos which contain little information about oscillations due to poor resolution of either neutrino direction (needed to reconstruct the path length) or energy; precisely the neutrinos which are excluded from the analysis [2], see e.g. [24].

The effects of uncertainties on absolute fluxes is fairly straightforward, a 10% change in hadron production or primary flux across the relevant regions of parameter space results in a 10% change in neutrino fluxes. The effects of uncertainties on various ratios of fluxes, such as up/down, or ν_μ/ν_e, is much less intuitive and also of considerable interest. The ratios are in principle much more stable against the uncertainties because any change affects the numerator and denominator in similar ways (e.g. in the ν_μ/ν_e ratio, both the ν_μ and ν_e flavoured neutrinos are mainly produced in association with muons, therefore an increase in e.g. pion production will increase the muon flux by a similar amount which will increase both ν_μ and ν_e fluxes by similar amounts). This cancellation is absolutely vital in extracting neutrino oscillation information from atmospheric neutrinos. Data analyses are constructed to take advantage of cancellation of uncertainties in the ratios.

The main challenge in estimating the uncertainties in the computed unoscillated neutrino fluxes is to assign errors to the different measurements which are taken as input to the

calculation. The dependence of the fluxes on the atmospheric density as a function of altitude, the details of muon energy loss in the atmosphere and the tracking in the Earth's magnetic field are found to be small [25]. The dominant sources of error are from uncertainties in hadron production and following this, uncertainties in the primary flux. We restrict ourselves to estimating errors from these two sources in this paper.

The hadron production uncertainty is due to the large regions of parameter space (incident parent total energy E_i, secondary total energy E_s (or equivalently, x_{lab}, defined as E_s/E_i), transverse momentum p_T, target atomic weight A, projectile, secondary particle type) which are only sparsely populated by measurements from accelerators. Since measurements of production of neutrons and π^0 are almost entirely absent, total energy conservation is not a strong constraint.

This sparse population of hadron production phase space also makes it difficult to assign uncertainties on the value which has been used. We proceed with a pragmatic approach which is described in detail in Sec. III, to summarize, we select a given number of regions into which to divide the phase space and then assign independent errors to each based on the amount of existing accelerator data in that region. In quite a number of cases, this requires assigning an error to the procedure of extrapolation in p_T, x_{lab}, E_i or target nucleus. This assignment has been done by us and is somewhat subjective. In all cases, it has been the intent to assign errors on the basis of the level of agreement between experimental measurements in a given region, or the amount of extrapolation into regions where measurements do not exist. The use of comparison between different models to assign errors has been avoided. The approach described in Sec. IV has been used to address the correlation which exists between any mismeasurement in one region of phase space with the other regions. To establish that this method is reasonable, several variations have been tried and are presented in Sec. VIII with a number of other crosschecks.

Primary flux measurements are challenging because a variety of experimental techniques are required to cover the large energy region of interest between 1 GeV and 10 TeV, the steeply falling flux as a function of energy makes calibration a critical issue and the experimental apparatus needs to be operated in a hostile environment on a balloon or spacecraft. However, several high-precision measurements of the primary flux now exist [26–28] which resolve the historical discrepancy in the earlier data. These errors are included in the uncertainty estimate in a similar way to the hadron production as described in Sec. V.

Following this, Sec. VI discusses the uncertainties obtained on the absolute fluxes, the type-ratios ν_μ/ν_e, $\nu_\mu/\bar{\nu}_\mu$, $\nu_e/\bar{\nu}_e$ and the directional ratios up/down and up/horizontal of both muon and electron type neutrinos. Since

most underground detectors are insensitive to lepton charge and therefore cannot distinguish neutrino and anti-neutrino, throughout this paper, the symbols ν_μ and ν_e are used to refer to the sum of neutrino and antineutrino fluxes except when explicitly used alongside a symbol for anti-neutrino, e.g. as in $\nu_\mu/\bar{\nu}_\mu$ or $\nu_\mu + \frac{1}{2}\bar{\nu}_\mu$. The paper continues with Sec. VII that classifies the uncertainties in the absolute fluxes and ratios according to which regions of hadron production phase space and primary flux are most responsible for the uncertainties. Various cross checks are presented in Sec. VIII and a limitation to the cancellation which is important when combining fluxes measured at different parts of the solar cycle into a ratio is shown in section IX. Finally, concluding remarks are given in section X.

II. PREVIOUS WORK

Several previous estimates of uncertainties have been made. Agrawal *et al.* [11] have extracted error estimates of spectrum weighted moments, such as

$$Z_{p\pi} = \int_0^1 \frac{1}{\sigma_{p\pi}} \frac{d\sigma_{p\pi}}{dx_{\text{lab}}} (x_{\text{lab}})^\gamma dx_{\text{lab}}. \qquad (1)$$

These arise naturally from an analytic calculation which is possible if the flux can be approximated by a power law dependence $E^{-(\gamma+1)}$ [29] which holds at high energies. The authors compare spectrum weighted moments obtained from data samples and from the hadron production models used in the calculation. They consider secondary pions and kaons and the ratio between pions and kaons, but do not consider how the uncertainty in π^+/π^- or K^+/K^- affects the ratios. Battistoni *et al.* [13] describe in detail the methods by which the FLUKA Monte-Carlo hadron production generator operates. The authors give many examples of cross checks between FLUKA predictions and data measurements, such as predicting [30] the measurements by AMS [26] from 320–390 km altitude of the backscattering of secondary particles from cosmic rays interacting in the atmosphere. They assign errors of ~10–15% on absolute fluxes and ~2–5% on the flavour ratios.

The Super-Kamiokande paper [1] describes the issues involved in the flux uncertainties carefully and includes estimates of the uncertainties based on comparison of the different calculations which have been done. The paper also uses input on uncertainties from [11,15,19] and the authors have made estimates of how much their unoscillated flux model is allowed to move. They assign errors on the ratio ν_μ/ν_e of ~3% for $E_\nu < 5$ GeV, increasing to 10% at 100 GeV. Errors on $\nu_\mu/\bar{\nu}_\mu$ and $\nu_e/\bar{\nu}_e$ are 5% below 10 GeV increasing to 25% and 10% above 100 GeV for $\nu_\mu/\bar{\nu}_\mu$ and $\nu_e/\bar{\nu}_e$ respectively. Errors on the up/down ratio are around 1 to 2%. The absolute normalization is a free parameter in the Super-Kamiokande oscillation fits reflect-

ing that the uncertainties on the absolute fluxes could be large.

Tserkovnyak *et al.* [14] have performed their calculation with different hadron production generators for comparison.

The disadvantage of any technique which compares models as the sole method of estimating uncertainties is the possibility of disagreements having been tuned away as a correction to any previous comparison between the models; i.e. there is the possibility that all the models are wrong in the same way.

It is possible to use the many measurements of muon fluxes as a validation of atmospheric neutrino flux predictions, a technique which is used by the authors discussed above and which gives a strong indication that the errors are in the range which they quote. It must be noted however that muon fluxes measured at a given altitude are much more sensitive than neutrino fluxes measured in underground detectors to uncertainties due to energy loss and atmospheric density. Muons observed at sea level are roughly 1% of all produced muons, while neutrino fluxes measure the total number of produced muons. The present work concentrates on propagating experimental uncertainties in hadron production and primary fluxes forward through the calculations of neutrino fluxes and does not use input from muon flux measurements.

III. HADRON PRODUCTION UNCERTAINTIES

The errors on the hadron production have been estimated using only experimental measurements which were available for the hadron interaction models used by current atmospheric neutrino analyses [1,2,4–6]. More extensive measurements covering a larger fraction of the phase space have recently become available from HARP [31] and NA49 [33,34]. Further measurements with carbon targets are expected soon from HARP, E910 [32], and MIPP [35].

The assignment of uncertainties to the different parts of the parameter space has been done on the basis of the availability of data and the amount of extrapolation required. This is described in detail in [25]. It has largely been done in a model independent way, but with a few guiding indicators. In particular, when the projectile energy is in the region where resonances can be excited, the production cross section varies rapidly across parameter space and is difficult to extrapolate. At higher energies, the particle production varies more smoothly (Feynman scaling).

Since only one neutrino from any given cosmic ray shower is ever detected, it is necessary to consider only single particle, inclusive hadron production as we track uncertainties through the calculation. We consider the reaction $pN \rightarrow \pi^\pm X$, where p is the projectile, N the target nucleus $\pi^\pm$ the particle of interest (a pion or kaon usually) and X represents the rest of the interaction products. In most of the discussion of this paper, the projectile is

a proton and the target is a light nucleus such as beryllium, carbon or aluminum, which can be extrapolated to nitrogen and oxygen, which are the targets in the atmospheric cascade.

When a shower develops, the initial cosmic ray undergoes several interactions in which the initial energy is split among the branches of the shower. Tracing backwards through the shower from the neutrino, through the ancestors to the original cosmic ray, one can define the branch along which any particular neutrino was produced. At some point along the branch, there is a meson ($\pi^{\pm}$, $K^{\pm}$ or K^0) which decays. The neutrino may be produced directly in this decay or via a muon. It is the distribution of energy, position on the globe and direction of these mesons which govern the neutrino fluxes. This meson will be referred to as "the decay meson".

To simplify, we have limited the study of hadron production uncertainties to the interaction in which the first meson in the branch has been produced (i.e. its parent was a baryon). We now discuss two aspects which have been neglected in the uncertainties due to this simplification. (1) It is possible in the branch that the first meson to be produced interacts and produces a subsequent string of hadrons before we reach the decay meson. This depends on the local atmospheric density and because of time dilation effects, is important only for higher energy mesons (above ~200 GeV for pions and 600 GeV for kaons). The secondaries of such interactions will be lower in energy, a region populated by a large number of directly produced decay mesons from lower energy cosmic rays, so the additional uncertainty because of such interactions is small. (2) The branch may contain a chain of interactions in which the initial cosmic ray baryon is converted into lower energy baryons before the decay meson is produced. This could happen both by near-elastic scatters or in higher multiplicity interactions. Some of these daughter baryons are neutrons and very few hadron production measurements concerning either the production of neutrons or interactions with neutron projectiles are available. Therefore all aspects of neutrons in cosmic ray showers are obtained from isospin arguments from proton measurements. The uncertainty associated with this simplification (2) requires separate study.

Figure 1 shows a map of the (E_i, E_s) phase space which is important for the production of neutrinos with energies appropriate to produce contained events in underground detectors and indicates the locations of hadron production experiments.

Engel, *et al.* [36] summarize the extent to which these measurements cover the third dimension of phase space, transverse momentum p_T. It is most important in atmospheric neutrino interactions to understand the p_T-integrated yields. Yields at specific values of p_T are less important since all p_T values are collected with the same probability in underground detectors (in contrast to
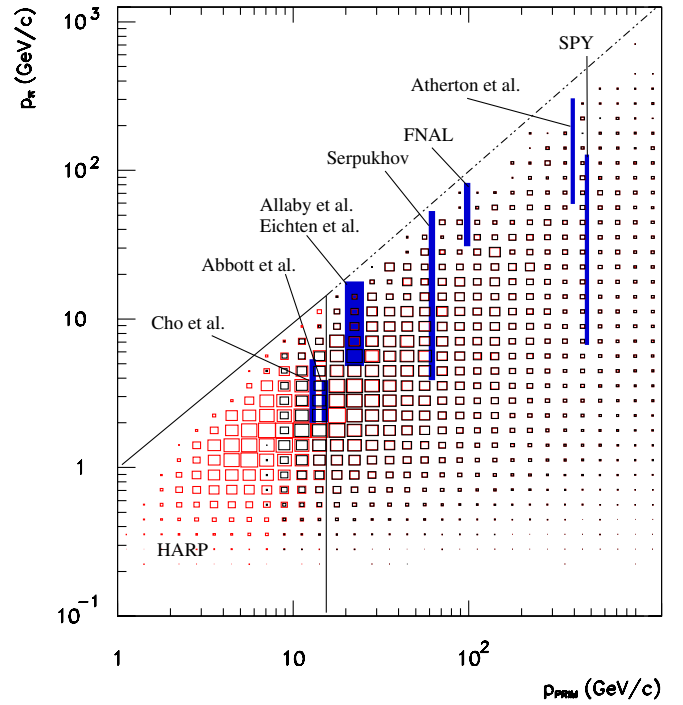

FIG. 1 (color online). Summary of measurements of single particle production yields as a function of primary energy and secondary energy. The bands for each experiment represent the range of primary and secondary particle energies where measurements exist for at least one value of p_T. The boxes on the plot show the contribution of the phase space to the generation of contained underground neutrino events as computed by the simulation. The outer (red) and inner (black) boxes indicate the extremes of geomagnetic field effects for high and low geomagnetic latitude, respectively.

accelerator beams where magnetic fields are used to focus specific regions of p_T to form the beam). Measurements over the whole p_T range are important to determine the integral.

Most of the experiments report yields for both signs of charged pions and charged kaons. We discuss the uncertainties on charged pion yields first and then kaon yields. The uncertainties assigned are summarized in Fig. 2. There is a series of measurements with primary energies around 20 GeV [37–39] with consistent measurements spread over as much as 80% of the p_T phase space [36], allowing the

FIG. 2. Uncertainties assigned to the production rate of charged pions (left) and charged kaons (right) as a function of x_{lab}. The uncertainties are shown for various ranges of incident particle energy E_i for interactions of protons on light nuclei.

hadron production to be determined without significant extrapolation. Above x_{lab} of 0.6, this coverage reduces to around 50% requiring some extrapolation. There is only one experiment with measurements between x_{lab} of 0.1 and 0.2 and no measurements at all when x_{lab} is below 0.1. We have therefore assigned errors of 5% in the region $0.2 < x_{\text{lab}} < 0.6$, (somewhat below the errors quoted by a single experiment, to account for the good agreement between measurements) and have increased the errors to 10% for $0.1 < x_{\text{lab}} < 0.2$ and to 30% for $x_{\text{lab}} < 0.1$ where extrapolation in x_{lab} is necessary. Extrapolation to very low x_{lab} is challenging due to the uncertainty of how large the role of resonances is. Above $x_{\text{lab}} = 0.6$, an error of 10% is assigned due to the more limited coverage of [37] in p_T for π^-. This procedure is described in detail in ref. [25].

Errors also include a contribution due to extrapolation between targets. The best solid target is carbon which like the major components of the atmosphere contains equal numbers of neutrons and protons. Unfortunately, none of the measurements [37–39] used carbon, but did measure with Be, B$_4$C and Al.

The same procedure has been followed for E_i ranges below 8 GeV and between 8 and 15 GeV where measurements are available at intermediate x_{lab} ranges but extrapolation is required for $x_{\text{lab}} > 0.6$. Extrapolation is also required for $x_{\text{lab}} < 0.2$ in the $E_i = 8$–15 GeV range. Errors have been assigned assuming that it is not possible to extrapolate between these different E_i ranges due to resonance effects. The range $E_i > 30$ GeV is where Feynman scaling is more effective and it is assumed that extrapolation in E_i is possible. The three most extensive measurements are Barton *et al.* [40] at 100 GeV (which includes a measurement with carbon), Atherton *et al.* [41] at 400 GeV and measurements by the SPY collaboration [42] at 450 GeV. Above this, proton-proton measurements exist in limited regions of phase space from the ISR. A general 15% uncertainty has been assigned to the production rates in the region $E_i > 30$ GeV because some extrapolation is needed between the measurements and the p_T coverage is limited from any one experiment. Since there are no measurements below $x_{\text{lab}} = 0.1$ and resonance production in target fragmentation could be uncertain, the uncertainty is increased to 30% in this region. To reflect the reliance on models to extrapolate to high energies, where experimental data from accelerators are unavailable, an energy dependent uncertainty u is added linearly to the 15% (or 30% for $x_{\text{lab}} < 0.1$) for interactions in which parents are above 500 GeV as follows.

$$u(E_i) = 12.2\% \times \log_{10}\left(\frac{E_i}{500 \text{ GeV}}\right), \qquad (2)$$

so $u(1 \text{ TeV}) = 4\%$, $u(10 \text{ TeV}) = 16\%$ and $u(100 \text{ TeV}) = 28\%$. u is not allowed to exceed 50% (which occurs at $E_i = 6$ PeV).

The same procedure was used to assign uncertainties to kaons based on charged kaon production measurements. The uncertainties which are assigned are shown in Fig. 2. The kaon uncertainties are applied to both the charged and neutral kaons in the Monte Carlo calculation even though the level of K^0 and $\bar{\text{K}}^0$ production is determined through isospin relationships in the models. Many of the experiments which measure pion production also measure charged kaons, however below $E_i = 15$ GeV there are very few kaon production measurements and so larger uncertainties have been assigned in this region. The same value of u as described above was added linearly to the 30% when $E_i > 500$ GeV (40% when $x_{\text{lab}} < 0.1$).

Although the role of the uncertainty of secondary nucleon production is not addressed in this study, it is worth noting that the uncertainties are especially large in the energy region around $E_i = 20$ GeV. Figure 15 of Ref. [43] shows a comparison between data and various Monte Carlos; the data sets disagree and the models do not follow the data.

The constraint imposed by overall energy conservation in the interaction may be used to limit the size of hadron production uncertainties provided the amount of energy carried away by neutral particles such as neutrons and π° is estimated. The energy conservation constraint has not been used in the current study because it is intended that the individual hadron production error assignments used here can be scaled as future improvements in the measurements are made.

IV. UNCERTAINTY REGIONS

In order to carry out an analysis of the results of combining uncertainties in different regions of phase space, we want to define a set of uncorrelated sources of uncertainty that can be varied independently. Referring to Fig. 3, we assume that shifts within each region are fully correlated while completely neglecting correlations between adjacent regions. This is of course unrealistic, but we minimize the distortion of reality by choosing the boundaries so that as far as possible the different regions correspond to different physical effects. Thus for pions, Regions A, D and G contain the central region of phase space which relates
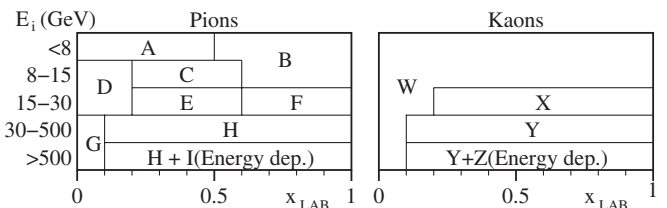

FIG. 3. Uncertainty sources for hadron production. The uncertainties which are applied are fully correlated within each region shown and completely uncorrelated between regions. The letters used to label each region are used on subsequent figures. The levels of uncertainties applied are shown in Fig. 2.

primarily to multiplicity, while regions B, C, E, F and H represent the fragmentation region in which the pion production is determined mainly by the valence quarks. Regions C and B are more closely connected to each other, as are E and F, but we treat them separately in order to track which regions of phase space would most benefit from more precise measurements.

For kaons, region W represents the very poorly measured part of phase where resonance production is important at low energy (below 15 GeV) and $s\bar{s}$ pair production in the central region is important at high energy. X and Y are used to represent associated production (a ΛK-pair) at high energy.

The energy dependent term in both pions and kaons at very high energies (Eq. (2)) is varied independently, represented by the regions I and Z.

The effect of changing the layout of these boundaries is found to have little effect on the uncertainty determination; we defer a discussion of this to section VIII on cross checks.

The approach chosen allows different regions of phase space shown in Fig. 3 in the (E_i, x_{lab}) plane to vary independently with the allowed 1σ variation shown in Fig. 2. Since both the K/π ratio and the K^+/K^- ratio are nearly as poorly measured as the K production itself, the K^+ and K^- production are varied entirely independently of each other and of the π production. An uncertainty for the π^+/π^- ratio of $\pm 5\%$ has been applied. We assume that the interaction can be considered as a combination of centrally produced *pairs* of pions which do not contribute to an uncertainty in the charge ratio and a 20% contribution to the uncertainty from projectile fragmentation. This is obtained by assuming that the projectile may be excited into a state with given isospin which subsequently decays to a nucleon and a single pion and evaluating the different possibilities.

The number of different uncertainty sources in our analysis is 18 in total (9 in pions, 4 in K^+, 4 in K^- and 1 representing the π^+/π^- ratio). It has been chosen to be roughly the same as the number of questions and worries in the model builder's minds. If the number of regions is too small (e.g. only 2 or 3), this describes a situation in which the shape of the hadron production is well defined, but the overall rate is unknown; in this case, the uncertainty cancels almost completely in the ratios of neutrino fluxes. If the number is too large (e.g. a few hundred) and all vary independently, this describes a situation in which there are large variations between local parts of the phase space and the uncertainties in adjacent regions average out and again underestimates the true uncertainty.

V. PRIMARY FLUXES UNCERTAINTIES

The primary flux uncertainties are incorporated into the uncertainties on the neutrino fluxes in a similar way to the hadron production uncertainties. Gaisser, Stanev, Honda,

TABLE I.   Summary of primary flux parameter variation.

Parameter	Proton fluxes	Nuclear fluxes
a (normalization)	1.49 ± 0.10	0.060 ± 0.004
b	2.15 ± 0.025	1.25 ± 0.03
c	-2.21 ± 0.02	-0.14 ± 0.02
d (index) <200 GeV/n	2.74 ± 0.01	2.64 ± 0.02
>200 GeV/n	2.74 ± 0.03	2.64 ± 0.04

and Lipari [44] (GSHL) have parameterized the primary fluxes as a function of energy in solar minimum conditions, based on a compilation of a large number of flux measurements. Measurements up to 200 GeV/n are possible using balloon or spacecraft mounted experiments. At higher energies, fluxes are determined by balloon borne emulsion-calorimeter techniques which are less precise. The GSHL parametrization gives the fluxes as follows

$$\Phi(E_{\mathrm{p}}) = a[E_{\mathrm{p}} + b\exp(c\sqrt{E_{\mathrm{p}}})]^{-d}, \qquad (3)$$

where E_{p} is the primary energy in GeV (in GeV/nucleon for nuclear cosmic rays) and $d = \gamma + 1$ is the differential spectral index. The parameters a, b, c, and d are chosen separately for the proton fluxes and for the sum of all the nuclear fluxes. The parameter d governs the most striking feature of the cosmic ray fluxes; the extremely steep falloff with energy.

The uncertainties are obtained by estimating the variation required in the parameters a to d to suitably cover the spread in the modern measurements. The values used are shown in Table I. The uncertainty on the parameter d is
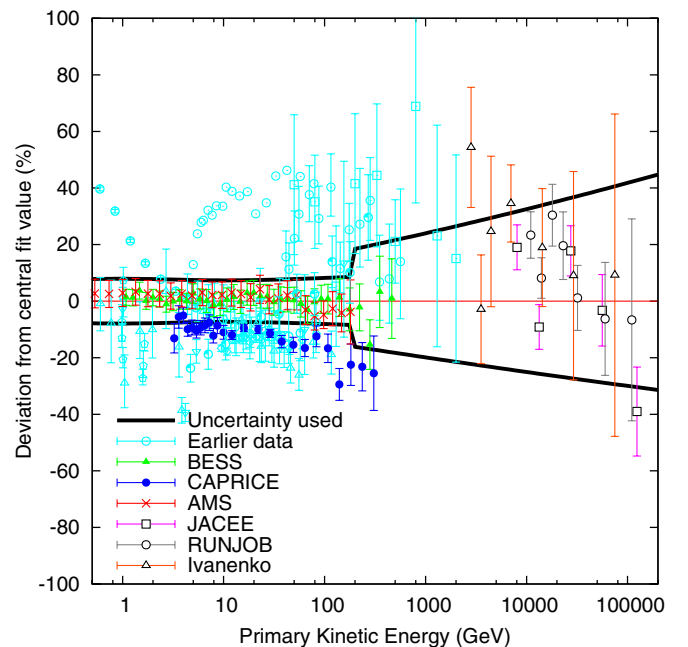

FIG. 4 (color online).   Comparison of proton flux measurements to the GSHL parametrization with parameters given in Table I as a function of energy. The lines show the uncertainties on the fluxes used in this paper.
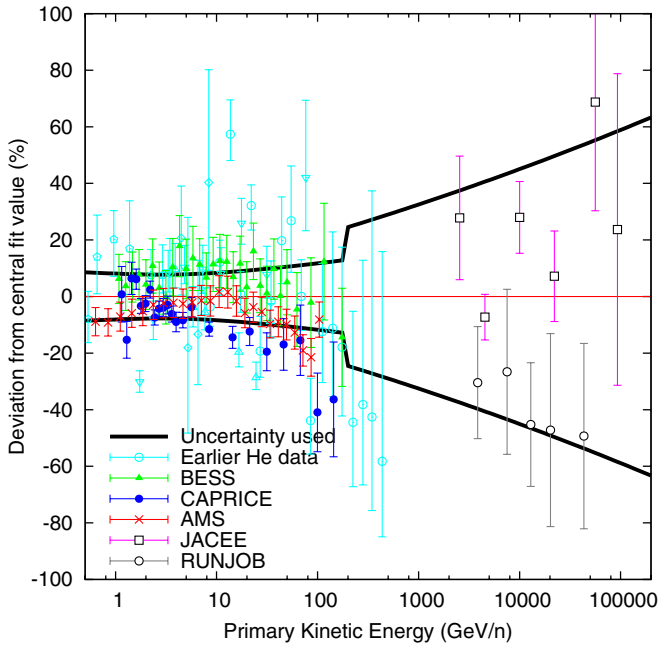
FIG. 5 (color online). Comparison of helium flux measurements to the GSHL parametrization with parameters given in Table I as a function of energy per nucleon. The lines show the uncertainties on the fluxes used in this paper.

increased by a factor of 3 for primaries above 200 GeV/n where the fluxes can not be measured with spectrometers.

The proton flux measurements are compared on Fig. 4 where the residual between the measurements and the above parametrization are plotted against cosmic ray energy. Historically, there was a discrepancy among earlier measurements of up to 50% in the important region between 10 and 100 GeV. Modern experiments are in much better agreement although the data of CAPRICE [28] is a little lower than AMS [26] and BESS [27] which agree with each other very well. Analogously to the hadron production, the proton flux uncertainties are applied by using four uncertainty sources to allow the changes to the parameters a, b, c, and d to be applied independently.

The primary cosmic ray flux contains nucleons which are bound in nuclei of various sizes. For this estimate of the errors, we have assigned errors to the fluxes to cover the spread in helium fluxes as shown on Fig. 5 and used these errors as four more uncertainty sources to represent the variation for all nuclei other than protons.

VI. ERROR ESTIMATES

The flux calculation proceeds by performing a Monte-Carlo calculation with the same simulation program as in Ref. [20] at 70 separate equally logarithmically-spaced energies between 1 GeV and 10 PeV and summing up the neutrinos which are produced; normalizing to the correct number of primary cosmic rays. To estimate the uncertainties, the calculation was repeated 26 times with each of the uncertainty sources described above (18 in hadron produc-

tion and 8 in primary flux) individually adjusted by 1σ to obtain the variation in neutrino flux as a function of neutrino energy, type and zenith angle for each of the changes. The hadron production adjustment is performed by weighting the neutrinos where the first meson is produced with the values of E_i and x_{lab} in the appropriate ranges. The total uncertainty in the neutrino flux is obtained by adding the deviations in the 26 calculated fluxes in quadrature. Similarly, to determine the error on a given flux ratio, the ratio is recalculated for each of the 26 changes and these deviations are added in quadrature.

The 1D approximation has been used to derive the error sensitivities presented in this paper. Although the 1D approximation affects the values of the fluxes, it is not expected to change the sensitivity of the fluxes to the uncertainties considered here.

Figure 6 uses the muon neutrino to antineutrino flux ratio averaged over all zenith angles as an example to illustrate the level to which the cancellation in ratios occurs. The uncertainties on the fluxes are presented in two ways, firstly the fluxes are shown with error bars representing the uncertainties. Note how the neutrino flux falls steeply with energy in the same way that the primary fluxes do. This paper will concentrate on the uncertainties, for a more detailed description of the features of the fluxes themselves, see e.g. [20].
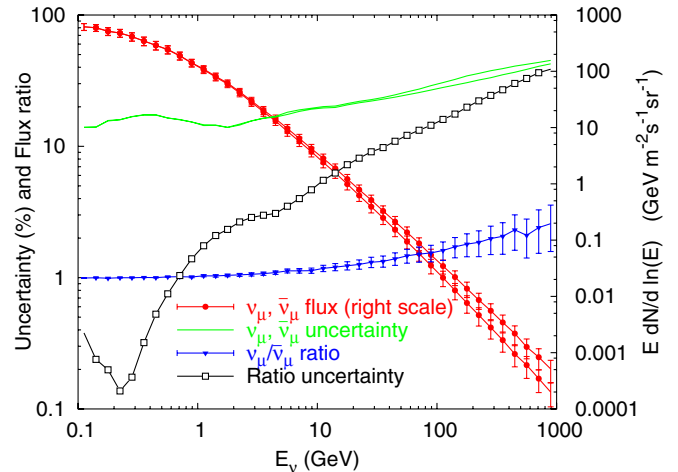

FIG. 6 (color online). Fluxes, flux ratios and uncertainties for muon neutrino/antineutrinos plotted as a function of neutrino energy. The muon neutrino and antineutrino fluxes are shown by (red) circular points, the upper line is ν_μ and the lower line is $\bar{\nu}_\mu$ plotted against the scale on the right axis, the error bars represent the uncertainty from hadron production and primary fluxes. All of the following curves are plotted against the scale on the left axis. The uncertainties (in percent) in the fluxes are shown again with the (green) lines with no points for ν_μ (lower line) and $\bar{\nu}_\mu$ (upper line). The ratio of ν_μ flux to $\bar{\nu}_\mu$ flux is plotted by the (blue) line with triangles and error bars indicating the estimated uncertainty in the ratio and the uncertainties in the ratio are shown in percent with the (black) line with square points. The large cancellation in the uncertainties in the ratio is apparent.

Figure 6 also shows the uncertainties plotted on their own (using the left scale), which is how they will be plotted in the later figures in this paper. They are around 15% at energies corresponding to contained neutrino events which is consistent with previous studies [11,13].

In constructing the ratio of muon-neutrinos to muon-antineutrinos, the computation takes account of the cancellation which occurs in the uncertainties, in this case because each muon in the atmosphere is associated with one neutrino and one antineutrino (all from the same parent pion) and so e.g. any overproduction of pions will tend to push both the numerator and denominator in the ratio upwards. The ratio of muon neutrino to antineutrino is shown on Fig. 6 (in blue) with downward triangle markers with error bars representing the uncertainty in the ratio. The uncertainty is also shown separately (as later plots in the paper will be shown). A large cancellation is seen at low energies and the error on the ratio is well below 1% around $E_\nu = 200$ MeV while the errors on the individual fluxes at this energy region is well above 10%, a cancellation of a factor of around 50. At higher energies, this cancellation becomes rapidly less powerful as some of the muons hit the ground and so the pions only produce one neutrino. Above 100 GeV there is hardly any cancellation at all.

Figure 7 presents the uncertainties on all three neutrino-type ratios averaged over all directions. The $\nu_\mu/\bar{\nu}_\mu$ ratio is as shown on Fig. 6. The $\nu_e/\bar{\nu}_e$ ratio does not show the same level of cancellation, since only a maximum of one electron neutrino is produced from each pion. The uncertainty on $(\nu_\mu + \bar{\nu}_\mu)/(\nu_e + \bar{\nu}_e)$ shows similar cancellation characteristics to $\nu_\mu/\bar{\nu}_\mu$ since a single muon contributes to both the numerator and denominator; the cancellation is large at low energies (where no muons hit the ground) because muons always produce neutrinos with both fla-
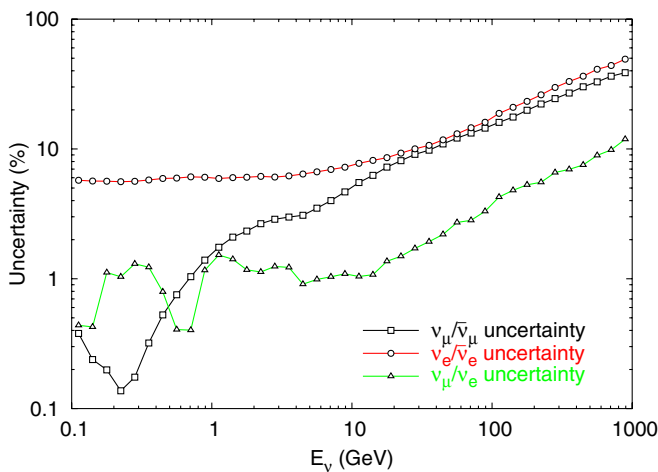
vours (in the ratio 2:1). At higher energies, the ratio increases, but not as fast as $\nu_\mu/\bar{\nu}_\mu$.

Figure 8 gives the variation of the neutrino-type uncertainties as a function of zenith angle for three different
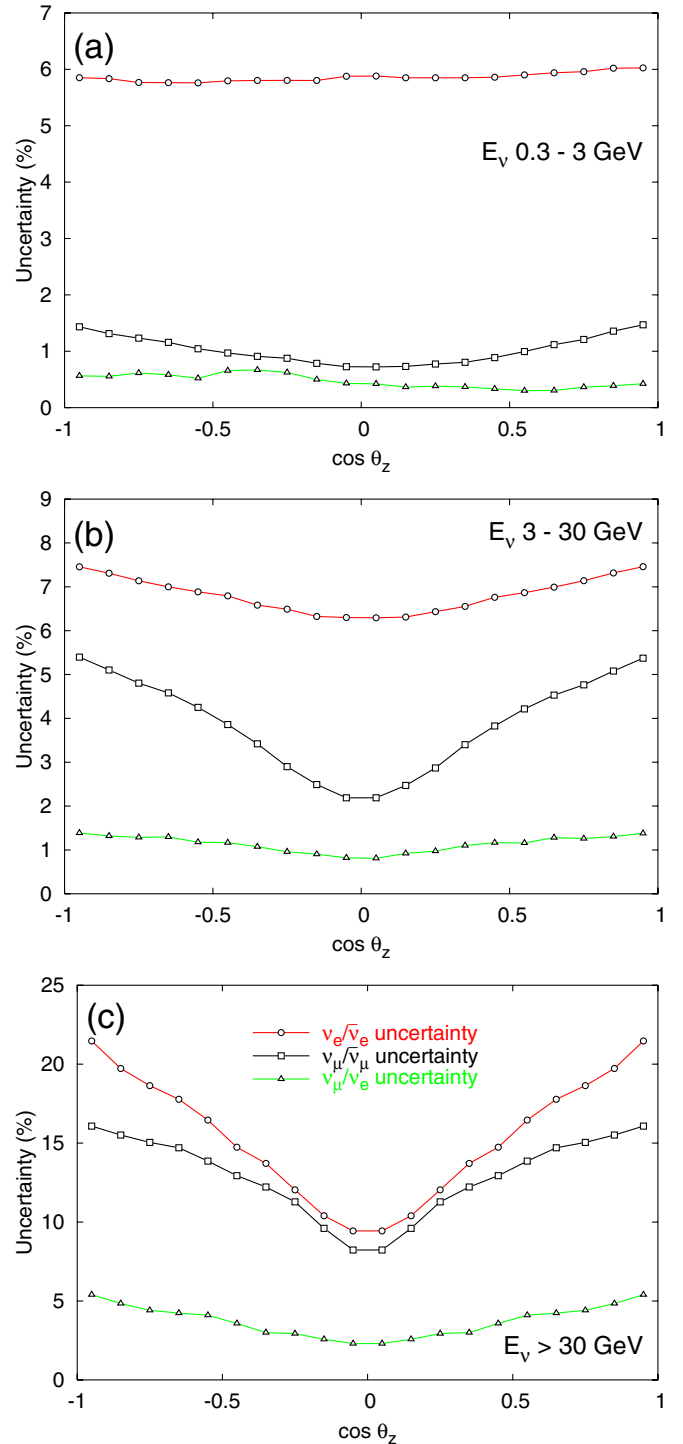

FIG. 8 (color online). Uncertainties in neutrino-type ratios as a function of zenith angle for (a) 0.3–3 GeV, (b) 3–30 GeV and (c) above 30 GeV neutrino energy ranges. $\nu_\mu/\bar{\nu}_\mu$ is shown with (black) lines with squares, $\nu_e/\bar{\nu}_e$ with (red) lines with circles and $(\nu_\mu + \bar{\nu}_\mu)/(\nu_e + \bar{\nu}_e)$ with (green) lines with triangles.

FIG. 7 (color online). Uncertainties in neutrino-type ratios as a function of neutrino energy. $\nu_\mu/\bar{\nu}_e$ is shown with (black) lines with squares, $\nu_e/\bar{\nu}_e$ with (red) lines with circles and $(\nu_\mu + \bar{\nu}_\mu)/(\nu_e + \bar{\nu}_e)$ with (green) lines with triangles.

neutrino energy ranges. At low energy, below $E_\nu = 3$ GeV, where the muons do not hit the surface, the uncertainty cancellation is good in all directions [Fig. 8(a)]. As shown in Fig. 8(b), at intermediate energies, the uncertainty cancellation disappears more rapidly for vertical neutrinos than for horizontal ones as the vertical muons hit the ground with lower energies (path length ~ 20 km) than horizontal ones (path length ~ 500 km). For neutrinos with energy above 30 GeV, the uncertainties on all three ratios are smaller by about a factor of 2 near the horizontal than near the vertical. The competition between interaction and decay of the mesons causes kaons to become more important at high energy. This occurs first near the vertical because the local atmospheric density where the cascade occurs is greater for vertical showers than horizontal ones. The large uncertainties in the ratios near the vertical reflect the relatively large uncertainties in kaon production.

Cancellation of uncertainties also occurs in ratios of neutrinos from different directions. These are summarized in Fig. 9 which presents up/down and up/horizontal ratios for electron type and muon type neutrinos (in each case $\nu + \bar\nu$). Since these represent neutrinos with (in principle) identical signatures in a detector but with different distances from the neutrino production site, these ratios are particularly useful for neutrino oscillation studies. For this study, the directions are defined as follows: up is neutrinos with $\cos\theta_z < -0.6$, horizontal is neutrinos with $|\cos\theta_z| < 0.3$ and down is neutrinos with $\cos\theta_z > 0.6$. The calculation has used the Kamioka detector site in Japan which is close to the geomagnetic equator (i.e. the low energy cosmic rays locally are suppressed compared to other points on the Earth).

The uncertainty in the up/down ratio cancels exactly in the region $E_\nu > 4$ GeV where the primary cosmic rays are above about 40 GeV and are too high in energy to be affected by the Earth's magnetic field. At these high energies, there is in principle no difference between any two
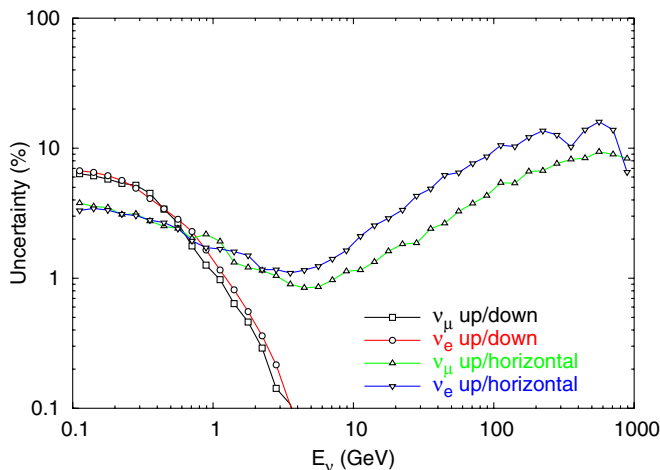
locations on the Earth and from a geometrical argument, the upward neutrinos have the same zenith angle (but traveling downwards) at the location of their production as at the detector. When $E_\nu < 4$ GeV, the geomagnetic cutoffs cause the spectrum of primary cosmic rays to be different for the up and the down neutrinos. Hence, different regions of hadron production phase space are selected and the cancellation in uncertainty is no longer exact. At low energies, the uncertainty in the up/down ratio is $\sim 7\%$ in agreement with earlier estimates [1,11]. The up/down uncertainties are the same for both muon and electron flavoured neutrinos.

Technically, in order to avoid statistical errors from the Monte-Carlo, it has been modified to generate neutrinos (in the 1D mode used in this calculation) in the downward direction and then to consider the neutrino as both downward and upwards by calculating the probability that the primary could penetrate the geomagnetic field and interact in the atmosphere in the appropriate location and direction for both directions. This means that Monte-Carlo statistical error on the up/down ratio comes only from the neutrinos which pass the cutoff calculation in one direction but not the other. The curves shown agree well with calculations where this modification is not implemented except for statistical fluctuations in the uncertainty estimates when E_ν is above 4 GeV.

The up/horizontal uncertainty is also shown on Fig. 9. Below $E_\nu = 4$ GeV, the features are caused by the same effect as the up/down ratio shown above. For $E_\nu > 4$ GeV, the errors no longer cancel. This is because of the different atmospheric density distribution as a function of slant depth which causes more meson reinteraction (rather than decay) for vertical cosmic rays than for horizontal ones. A pion which does not interact has a chance to produce a high energy neutrino, whereas one which interacts will produce a neutrino in a lower energy bin where there are many neutrinos from lower energy cosmic rays. Therefore the up/horizontal ratio at high energies is uncertain because meson reinteraction causes different regions of phase space to be emphasized.

VII. CONTRIBUTIONS TO THE UNCERTAINTY

The technique allows the contributions from the individual uncertainties which have been inserted to be compared. It is interesting to identify which uncertainties have the largest effect on any given quantity. These are shown in Figs. 10–13. The lines on all these plots are the same and are described in the caption to Fig. 10. The lines with symbols which are either solid or with the line going through them (A–I) are the pion uncertainties. The line with crosses (Chg) is the line representing the pion charge ratio uncertainty (for all phase space regions). The lines with symbols which over-stamp the line (W–Z) are the uncertainties from kaons. Each of the four lines W–Z represents the combination (quadrature sum) of two inde-

FIG. 9 (color online). Uncertainties in directional ratios as a function of neutrino energy.

Key:

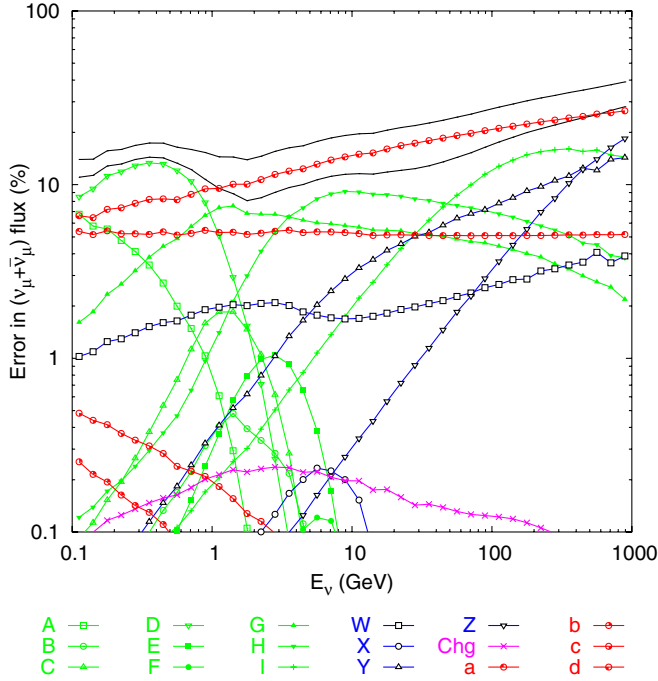|					
A	D	G	W	Z	b
B	E	H	X	Chg	c
C	F	I	Y	a	d

FIG. 10 (color online). Breakdown of flux uncertainties (shown here for angle averaged muon neutrinos) with different regions of hadron production as a function of neutrino energy. The capital letters in the key correspond with the hadron production uncertainty zones in Fig. 3 (green for π, blue for K) and the one labeled "Chg" represents the pion charge ratio uncertainty. The lower case (red) letters in the key correspond to variation of the flux parameters in Table I. See text for more information. The topmost thick (black) line with no points is the total error on the flux and the lower line of the same style is the total hadronic error (i.e. excluding the uncertainty from the primary flux).

pendent uncertainties for positive and negative kaons. The phase space regions corresponding to all these lines is summarized in Figs. 2 and 3. The lines with quartered circle symbols (a–d) correspond to the uncertainties on the primary flux parameters as given in Table I. Each line is the combination of the proton and all-nuclei contribution to the uncertainty.

Figure 10 shows the breakdown of uncertainties for the muon neutrino flux (angle averaged). No single source of error dominates. Above 1 GeV the primary flux uncertainty (in particular the value of the spectral index d) is important. The pion hadron production regions D, G, H, and I are important at, respectively, higher neutrino energies. The kaon uncertainties are not an important effect except at the very highest energies.

The three parts of Fig. 11 show the breakdown in uncertainties of the angle averaged neutrino-type ratios. The level of cancellation is different for the different error contributions and different for each of the three ratios. In no case does the primary flux contribution play a major role. The $(\nu_\mu + \bar{\nu}_\mu)/(\nu_e + \bar{\nu}_e)$ ratio shown in Fig. 11(a) is mostly affected by the pion production at low energy.
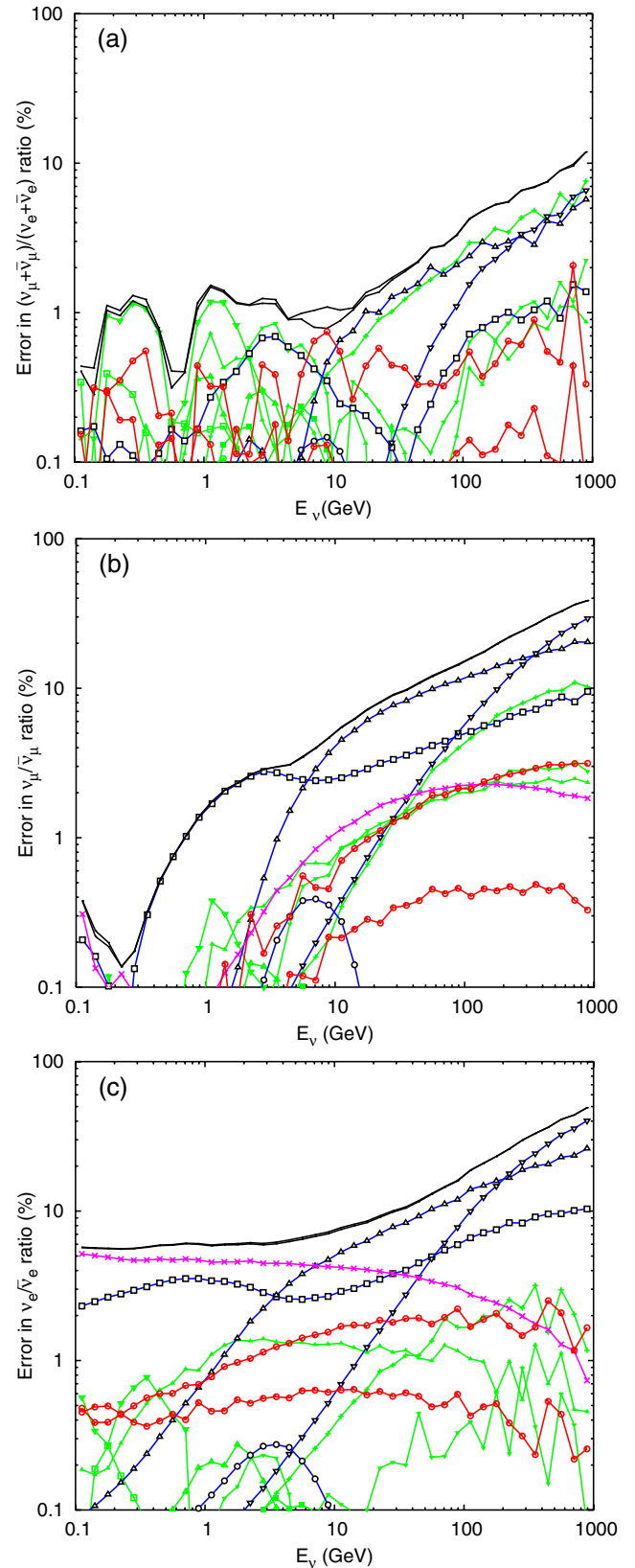

FIG. 11 (color online). Breakdown of uncertainties in flavor ratios with different regions of hadron production, shown as a function of neutrino energy. (a) $(\nu_\mu + \bar{\nu}_\mu)/(\nu_e + \bar{\nu}_e)$ ratio (b) $\nu_\mu/\bar{\nu}_\mu$ ratio and (c) $\nu_e/\bar{\nu}_e$. Key as in Fig. 10.

There are Monte-Carlo statistical effects in the uncertainties below about 0.3%. Figure 11(b) shows the $\nu_\mu/\bar\nu_\mu$ ratio which shows that the main uncertainties are caused by kaon production. We have perhaps been a bit pessimistic in assigning completely separate errors to K^+ and K^- production, however this reflects the different nature of the production of ΛK^+ and $K^+ K^-$ pairs. The breakdown in $\nu_e/\bar\nu_e$ uncertainties is shown in Fig. 11(c). Since only one electron type neutrino is produced for each pion and whether it is a neutrino or antineutrino is almost completely defined by the sign of the pion, this error is dominated by the pion charge ratio error assignment. We inserted an error on π^+/π^- of 5% and the error on $\nu_e/\bar\nu_e$ is essentially 5%. At higher energy ($E > 10$ GeV), kaon production begins to dominate the error budget as the Ke3 decay becomes the principal source of electron neutrinos.

Similarly Fig. 12 shows the breakdown in up/down ratio uncertainties for muon type neutrinos. The breakdown of the errors in up/down ratios for electron neutrinos is almost identical. The largest source of errors comes from hadron uncertainty source D followed by A; i.e. the hadron production regions at low x_{LAB}. The recent hadron production measurements cover this region, so the precision to which this ratio can be predicted should improve.

Figure 13 shows the up/horizontal flux ratio uncertainty breakdown for muon type neutrinos. At low energies, the contributions are similar to the up/down ratios. At high energies, all the uncertainty sources G, H, I, W, Y, and Z representing the uncertainties in hadron production with high energy parent particles are present, indicating that the different slant depth has caused a reduction in the cancellation of uncertainties.

FIG. 13 (color online). Breakdown of uncertainties in up/horizontal ratio, key as in Fig. 10.

The breakdown for electron type neutrinos in the up/horizontal ratio is similar with somewhat higher contributions from each of the hadron production uncertainty sources as shown on Fig. 9.

VIII. CROSS CHECKS

To check the stability of the uncertainty estimates presented in this paper, they were recalculated a number of times to quantify the effects of modifications. First, the layout of the uncertainty sources within the hadron production phase space was changed in three different ways. The effect on the ν_μ/ν_e ratio is shown in Fig. 14. In all three cases, the size of the uncertainties themselves were
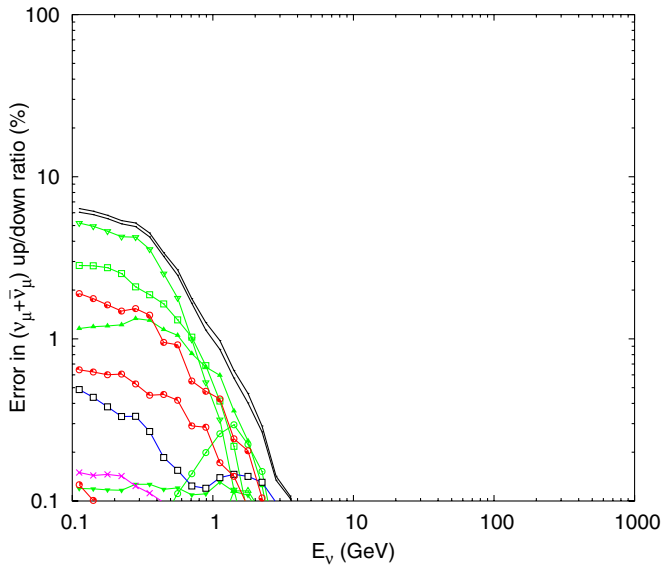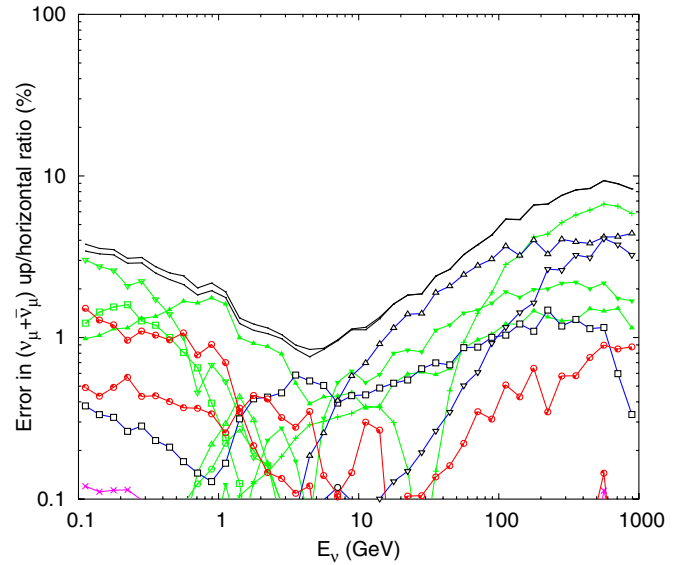

FIG. 12 (color online). Breakdown of uncertainties in up/down ratio for muon neutrinos, shown as a function of neutrino energy, key as in Fig. 10.
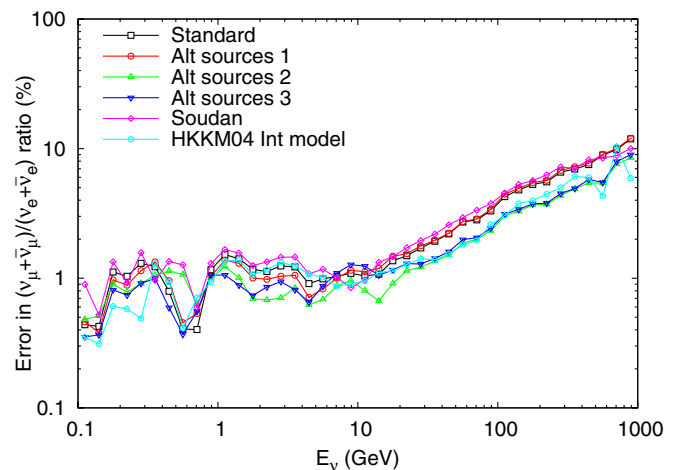

FIG. 14 (color online). Stability of the uncertainty estimates as a function of different choices of uncertainty sources ((1), (2), (3)), detector location (Soudan) and base hadron production generator.

E_i (GeV)	Pions						Kaons					
<8	01		02		03	04	01		02		03	04
8–15	05	06	07	08	09	10	05	06	07	08	09	10
15–30	11	12	13	14	15	16	11	12	13	14	15	16
30–500	17	18	19	20	21	22	17	18	19	20	21	22
>500	23	24 + 25(Energy dep.)					23	24 + 25(Energy dep.)				

0   0.5 x_{LAB} 1   0   0.5 x_{LAB} 1
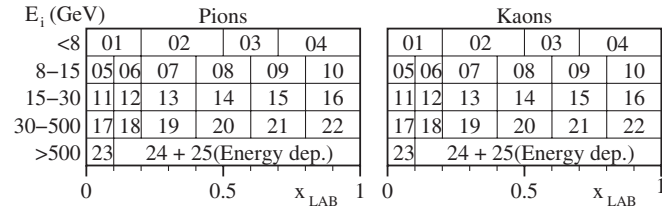
FIG. 15. Uncertainty sources used in the alternative 2 hadron production weighting scheme. The sources 01–25 allow more independence to different values of x_{lab} than the standard scheme and have full correlation between pions and kaons in the same region of (E_i, x_{lab}).

maintained the same as in the standard calculation as shown on Fig. 2. Alternative 1 divides up the phase space in the same way as the standard uncertainty sources shown on Fig. 3 but to reflect that the uncertainties in the measurements are also present in the regions where they are extrapolated, each region of (E_i, x_{lab}) is influenced by up to two separate sources added in quadrature, the first is at the level of a region where measurements are made and the second reflects the additional error we added to account for extrapolation. For example, the region 8 GeV $< E_i <$ 15 GeV and $x_{lab} < 0.2$ is comprised of an uncertainty source with 10% uncertainty reflecting the measurement error and 28% due to extrapolation leading to a total error of 30%.

Alternative 2 rearranges the uncertainty sources to be more finely divided in x_{lab} and uses the same uncertainty sources for pions and kaons. It is shown in Fig. 15. Similarly, alternative 3, shown in Fig. 16 divides phase space more finely in E_i. All three schemes include the uncertainty sources for the primary fluxes and the π^+/π^- ratio. Alternative 1 handles the K^+/K^- in a similar way to the standard method and alternatives 2 and 3 include the K^+/K^- ratio uncertainty with a single source. As seen on Fig. 14, the uncertainty on the ν_μ/ν_e ratio is independent of which scheme is used. This is also true in general for the other ratios.

Figure 14 also shows two other cross checks which do not significantly affect the error estimation. The uncertainty analysis was run with a different detector location,
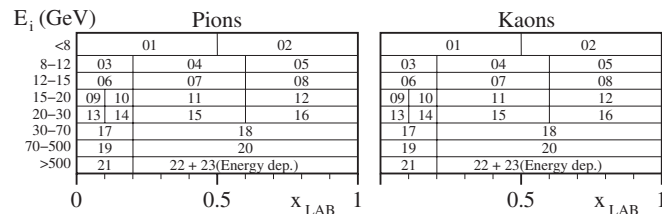
at Soudan in North America near one of the geomagnetic poles.

Since the analysis operates by applying weights to different regions of phase space it could give misleading results if, for example, part of the phase space is not used at all by the hadron production generator. We therefore repeated the analysis using the hadron production generator from the HKKM04 calculation [19] to verify that the same results were obtained as shown on Fig. 14.

A further cross check was to perform the combination of errors from different hadron production regions using a statistical method. The standard method moves each uncertainty source by 1σ, computes the movement of each ratio and adds the effects of each uncertainty source in quadrature. The statistical method performs 500 calculations each with randomly assigned uncertainties to all the uncertainty sources. The error on the fluxes and ratios was then determined from the widths of the distribution of the 500 different results. This method is equivalent and gave identical results within the limits of Monte-Carlo statistical fluctuations.

IX. SOLAR WIND

As seen in the distributions above, the uncertainties in flux ratios can be reduced significantly by cancellations. So far, all ratios shown assume that the ratios which are formed are taken simultaneously, i.e. no uncertainty is added if the two components of a ratio were taken at different times in the solar cycle where the solar wind changes the primary spectrum below cosmic ray energies of ~ 10 GeV. The MINOS experiment [6] is situated in the Soudan iron mine in Northern Minnesota, USA at the same location as the Soudan-2 experiment. Ref. [6] which studies muon flavoured neutrinos uses ν_e data from Ref. [4] to normalize the unoscillated fluxes from the Monte-Carlo calculation [20]. Since the Soudan-2 data and the MINOS

E_i (GeV)	Pions						Kaons					
<8	01			02			01			02		
8–12	03		04		05		03		04		05	
12–15	06		07		08		06		07		08	
15–20	09	10	11		12		09	10	11		12	
20–30	13	14	15		16		13	14	15		16	
30–70	17		18				17		18			
70–500	19		20				19		20			
>500	21		22 + 23(Energy dep.)				21		22 + 23(Energy dep.)			

0   0.5 x_{LAB} 1   0   0.5 x_{LAB} 1

FIG. 16. Uncertainty sources used in the alternative 3 hadron production weighting scheme. The sources 01–23 allow more independence to different values of E_i than the standard scheme and have full correlation between pions and kaons in the same region of (E_i, x_{lab}).
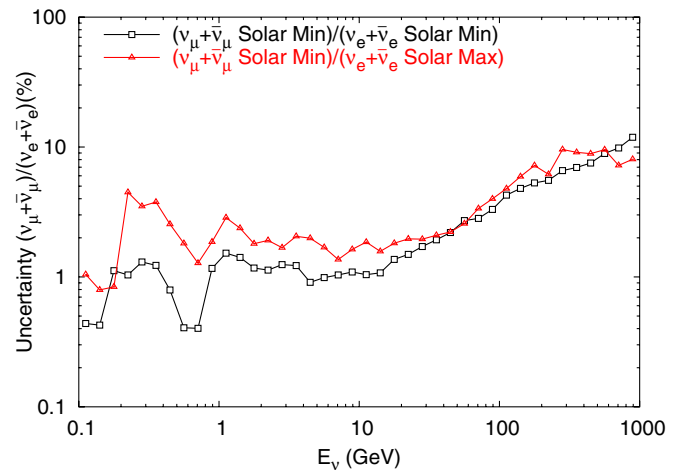

FIG. 17 (color online). Increase in muon neutrino to electron neutrino flux uncertainty when comparing fluxes from different parts of the solar cycle at Soudan.

data are taken at different parts of the solar cycle, the large cancellation in the ν_μ/ν_e ratio shown in Fig. 7 is not so exact. Figure 17 compares the uncertainty on the ν_μ/ν_e ratio between the standard calculation and one in which the ν_μ is taken at solar minimum conditions and the ν_e at solar maximum conditions. The uncertainty cancellation is not so good and is about 2.5% averaged over the energy region appropriate for the MINOS data sample.

X. CONCLUSIONS

A detailed survey of the main uncertainties involved in the computation of the production of neutrinos in the atmosphere has been presented. The major contributions which come from hadron production and the primary fluxes have been addressed. Regions where uncertainties exist and the amount of uncertainty in each region have been assigned based on the data which exists and not on any agreement or otherwise between different models (which may have been initially tuned on the same data or compared and adjusted to enhance agreement). An attempt to account for correlations of uncertainties across hadron production phase space has been employed and variants tested showing that the main conclusions of this paper do not depend on the particular scheme used.

The uncertainties on the fluxes are around 15% in agreement with previous evaluations. There is considerable cancellation of uncertainty when taking ratios of fluxes, either from different directions or of different neutrino types. These are of similar size to previous estimates [1,11,13], but are found to vary considerably with neutrino energy.

The breakdown of the uncertainties reveals that there is no single hadronic source of uncertainty which dominates. The production of pions at low energy which is currently being measured by several modern experiments is most important in the up/down and up/horizontal ratios for contained neutrinos. The knowledge of kaon production is important even for neutrinos as low as 4 GeV, particularly in the muon neutrino to antineutrino ratio.

As described in the paper, the method of assigning and applying the hadron production uncertainties to this problem is not unique or complete. One major omission with this method is that we have only included uncertainty at one point along the path to production of the neutrino, namely, at the production of the first mesonic ancestor of the neutrino. Another potential source of uncertainty is in the baryonic part of the shower. A primary proton may undergo several soft elastic or near elastic collisions, on its journey to the collision where the decay meson is produced. Low energy proton production is especially badly measured and models disagree considerably [43]. In addition, data on neutron production and also on interactions with neutron parents are very scarce.

The large degree of cancellation in the flux ratios, in particular, seen in the primary fluxes gives us encourage-

ment that these baryonic shower uncertainties are not going to be a major effect. Since they occur upstream of the hadron uncertainties we consider, they could be represented as an increase in flux uncertainty by redefining 'flux' to mean the spectrum of the baryons at the point of production of the first-meson.

The cancellations in uncertainties in flux ratios are a central part of any analysis of neutrino oscillation using cosmic rays. This study shows the details of this cancellation as a function of neutrino energy and for the first time identifies the sources of the uncertainties which remain. There are two major effects which are identified in the direction ratios which cause the cancellation to be incomplete.

The first effect is observed when the numerator and denominator of the ratio originate from cosmic rays which have different geomagnetic effects. This causes some regions of hadron production phase space to be only included in either the numerator or the denominator, so the uncertainty of that part of hadron production phase space does not cancel. This is apparent in the up/down ratio at low energy shown on Fig. 9. At high energy, where the cosmic rays are not removed by the geomagnetic field, the cancellation in the up/down ratio is exact.

The second effect is that if the slant depth in the atmosphere is different for the numerator and denominator (e.g. the up/horizontal ratio, but this applies to comparing any two different general zenith angle directions), then the balance between meson decay and interaction is different and cancellation is incomplete. This is illustrated on Fig. 18 which compares the usual up/horizontal uncertainty with one where all geomagnetic field effects have been removed. At low energy, the uncertainty is zero since all directions are now equivalent, but at higher energy, the uncertainty is as large as in the full uncertainty calculation.
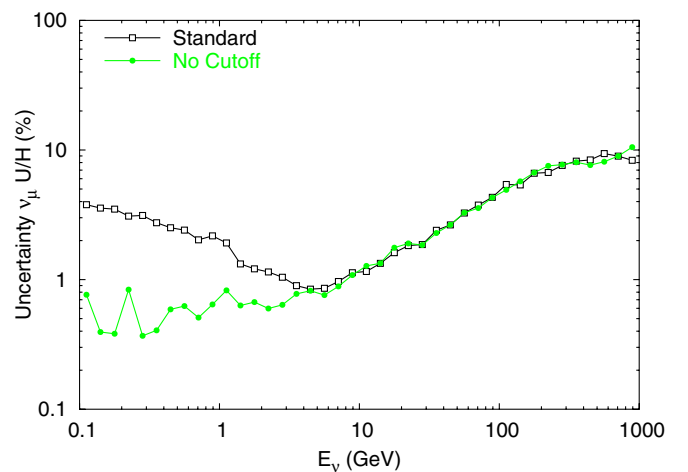

FIG. 18 (color online). Line with open squares shows the standard uncertainty in the up/horizontal ν_μ flux ratio and line with closed circles the uncertainty with the effect of the Earth's magnetic field removed.

[1] Y. Ashie *et al.* (Super-Kamiokande), Phys. Rev. D **71**, 112005 (2005).

[2] Y. Ashie *et al.* (Super-Kamiokande), Phys. Rev. Lett. **93**, 101801 (2004).

[3] Y. Fukuda *et al.* (Kamiokande), Phys. Lett. B **335**, 237 (1994).

[4] W. W. M. Allison *et al.* (Soudan-2), Phys. Rev. D **72**, 052005 (2005).

[5] M. Ambrosio *et al.* (MACRO), Eur. Phys. J. C **36**, 323 (2004).

[6] P. Adamson *et al.* (MINOS), Phys. Rev. D **73**, 072002 (2006).

[7] E. Aliu *et al.* (K2K), Phys. Rev. Lett. **94**, 081802 (2005).

[8] S. N. Ahmed *et al.* (SNO), Phys. Rev. Lett. **92**, 181301 (2004).

[9] S. Fukuda *et al.* (Super-Kamiokande), Phys. Lett. B **539**, 179 (2002).

[10] T. Araki *et al.* (KamLAND), Phys. Rev. Lett. **94**, 081801 (2005).

[11] V. Agrawal, T. K. Gaisser, P. Lipari, and T. Stanev, Phys. Rev. D **53**, 1314 (1996).

[12] M. Honda, T. Kajita, K. Kasahara, and S. Midorikawa, Phys. Rev. D **52**, 4985 (1995).

[13] G. Battistoni *et al.*, Astropart. Phys. **12**, 315 (2000).

[14] Y. Tserkovnyak, R. Komar, C. Nally, and C. Waltham, Astropart. Phys. **18**, 449 (2003).

[15] G. Battistoni, A. Ferrari, T. Montaruli, and P. R. Sala, Astropart. Phys. **19**, 269 (2003).

[16] J. Wentz *et al.*, Phys. Rev. D **67**, 073020 (2003).

[17] J. Favier, R. Kossakowski, and J. P. Vialle, Phys. Rev. D **68**, 093006 (2003).

[18] Y. Liu, L. Derome, and M. Buenerd, Phys. Rev. D **67**, 073022 (2003).

[19] M. Honda, T. Kajita, K. Kasahara, and S. Midorikawa, Phys. Rev. D **70**, 043008 (2004).

[20] G. D. Barr, T. K. Gaisser, P. Lipari, S. Robbins, and T. Stanev, Phys. Rev. D **70**, 023006 (2004).

[21] J. Hosaka *et al.* (Super-Kamiokande), hep-ex/0604011.

[22] T. Kajita and K. Okumura, *Proceedings of the 5th RCCN Workshop on Sub-Dominant Oscillation Effects in Atmospheric Neutrino Experiments* (Universal Academy Press, Tokyo, 2005).

[23] P. Lipari, Astropart. Phys. **14**, 153 (2000).

[24] G. Barr, Nucl. Phys. B, Proc. Suppl. **143**, 89 (2005).

[25] S. Robbins, D. Phil Thesis, University of Oxford, UK, 2004 [Report No. CERN-THESIS-2005-005].

[26] M. Aguilar *et al.* (AMS), Phys. Rep. **366**, 331 (2002).

[27] T. Sanuki *et al.* (BESS), Astrophys. J. **545**, 1135 (2000).

[28] M. Boezio *et al.* (CAPRICE), Astropart. Phys. **19**, 583 (2003).

[29] T. K. Gaisser, *Cosmic Rays and Particle Physics* (Cambridge University Press, Cambridge, England, 1990).

[30] P. Zuccon *et al.*, Astropart. Phys. **20**, 221 (2003).

[31] M. G. Catanesi *et al.* (HARP), Nucl. Phys. **B732**, 1 (2006).

[32] J. Link *et al.*, in preparation.

[33] C. Alt *et al.* (NA49), Eur. Phys. J. C **45**, 343 (2006).

[34] C. Alt *et al.* (NA49), hep-ex/0606028.

[35] Y. Fisyak *et al.*, The MIPP experiment, proposal 907, Fermilab, www.fnal.gov (2000).

[36] R. Engel, T. K. Gaisser, and T. Stanev, Phys. Lett. B **472**, 113 (2000).

[37] T. Eichten *et al.*, Nucl. Phys. **B44**, 333 (1972).

[38] J. V. Allaby *et al.*, CERN Yellow Report No. 70-12, 1970.

[39] T. Abbott *et al.* (E-802), Phys. Rev. D **45**, 3906 (1992).

[40] D. S. Barton *et al.*, Phys. Rev. D **27**, 2580 (1983).

[41] H. W. Atherton *et al.*, CERN Yellow Report No. 80-07, 1980.

[42] G. Ambrosini *et al.* (NA56/SPY), Eur. Phys. J. C **10**, 605 (1999).

[43] T. K. Gaisser and M. Honda, Annu. Rev. Nucl. Part. Sci. **52**, 153 (2002).

[44] T. K. Gaisser, T. Stanev, M. Honda, and P. Lipari, Proceeding of the 27th International Cosmic Ray Conference (ICRC 2001), Hamburg, Germany, 2001, 2001.